Journal of Applied Polymer Science

Fabrication of alumina based electrically conductive polymer composites

QuratulAin Nadeem,[1] Muhammad Rizwan,[2] Rohama Gill,[1] Muhammad Rafique,[2] Muhammad Shahid[2]
[1]Department of Environmental Sciences, Fatima Jinnah Women University, Rawalpindi 46000, Pakistan
[2]Department of Chemistry, Quaid-i-Azam University, Islamabad 45320, Pakistan
Correspondence to: Rohama Gill (E-mail: rohama_gill@hotmail.com)

ABSTRACT: Novel electrically conductive composites were synthesized by incorporating Cu coated alumina (Cu-Al_2O_3) powder prepared *via* electroless plating technique as filler (0–21wt %) into polystyrene-*b*-methylmethacrylate (PS-*b*-PMMA) and polystyrene (PS) matrices. XRD analysis depicted maximum Cu crystallite growth (26.116 nm~ plating time 30 min) onto Al_2O_3 along with a significant change in XRD patterns of composites with Cu-Al_2O_3 inclusion. SEM–EDX analyses exhibited uniform Cu growth onto Al_2O_3 and confirmed presence of Cu, Al, Pd in Cu-Al_2O_3, and C, O, Al, Cu, and Pd in PS-*b*-PMMA and PS composites. Increasing filler loadings exhibited increased electrical conductivity (5.55×10^{-5}S/cm for PS-*b*-PMMA; 5.0×10^{-6}S/cm for PS) with increased Young's modulus (1122MPa for PS-*b*-PMMA; 1053.9MPa for PS) and tensile strength (27.998MPa for PS-*b*-PMMA; 30.585MPa for PS) and decreased % elongation. TGA demonstrated increased thermal stability and DTG revealed two-step degradation in composites while DSC depicted pronounced increment in T_g of Cu-Al_2O_3/PS-*b*-PMMA with increased filler loading. © 2015 Wiley Periodicals, Inc. J. Appl. Polym. Sci. **2016**, *133*, 42939.

KEYWORDS: composites; glass transition; mechanical properties; polystyrene; thermogravimetric analysis

Received 11 May 2015; accepted 13 September 2015
DOI: 10.1002/app.42939

INTRODUCTION

With increasing technological advances, polymers and ceramic materials have been extensively used due to the tremendous advantages of such materials in energy conservation and consumption. One of such uses is to fabricate electrically conductive polymer composites by incorporating metallic particles/flakes including Ag, Cu, Au, etc. as fillers into insulating polymers.[1] However, the high cost and density of metal fillers diverted the attention towards comparatively low cost and less dense fillers with increased efficiency and durability when subjected to real life applications.[2,3]

In the field of metallic coating and conductive composites, there are various materials that have been studied and used for the production of conductive composites, such as electrodeposition technique to synthesize zirconia-poly(diallyldimethylammonium chloride) (PDDA) composite films[4]; chemical vapor deposition (CVD) to deposit ultra thin graphene layers on polycrystalline Ni surface[5]; physical vapor deposition (PVD) to grow hexagonal bismuth tri-iodide platelets[6]; chemical oxidative polymerization to fabricate Fe_3O_4/polyaniline (PANI) nanocomposites[7] and multi-walled carbon nanotubes (MWCNTs)-core/thiophene polymer–sheath composites[8]; electrospinning to prepare poly(3,4-ethylene dioxythiophene) (PEDOT)/poly(lactide-co-glycolide) (PLGA) micro and nano fibers/tubes[9]; ultrasonic irradiation method to prepare SiO_2/Poly (3-aminophenylboronic acid) nanocomposites[10]; *in situ* polymerization to synthesize PANI/CNTs nanocomposites[11] and polyimide/graphene nanocomposites[12] etc.

Among these processes, electrolytic plating[13] has been a traditional and conventional process used since long. However, in this process, the substrate must be a conductive material. Electroless (EL) plating is yet another option that has offered metallization over a range of substrates including conductors, semiconductors, and even on non-conductors that was not possible *via* conventional electroplating technique. Its simplicity in design and operation, cost effectiveness and requirement of low temperature conditions to put together conductive fillers with insulating polymers to synthesize electro-thermally conductive polymer matrix composites.[14] The selection of deposition technique, i.e., EL deposition render a unique approach for the fabrication of high strength electrically conductive composites by metalizing a non-conductive substrate, alumina with copper which is then used for the first time as filler for block copolymer (PS-*b*-PMMA) and homopolymer (PS) matrices. The prepared composites may have potential to be used as electromagnetic interference (EMI) and electrostatic dissipative (ESD)

© 2015 Wiley Periodicals, Inc.

shields,[15] embedded heat skins for heat dissipation in microelectronics,[16] and electrochemical sensors for biomedical applications[17] etc.

EXPERIMENTAL

Materials

All the chemicals and reagents used in this study were of analytical grade and used without further purification including Fluka Chemika [Aluminium oxide (Al_2O_3)], Riedel-de Haen [Nitric acid (HNO_3 37%), Copper sulphate penta hydrate ($CuSO_4.5H_2O$), Potassium sodium tatrate ($KNaC_4H_4O_6{\cdot}4H_2O$)], Merck [Hydrochloric acid (HCl 37%), and hydrofluoric acid (HF)], Scharlau [Sodium hydroxide (NaOH)], Fisher Scientific [tetrahydrofuran (THF)], Sigma Aldrich [Sodium chloride (NaCl), Stannous sulphate ($SnSO_4$), Palladium chloride ($PdCl_2$), Stannous chloride ($SnCl_2.2H_2O$), Ethylenediaminetetraacetic acid disodium salt ($C_{10}H_{14}N_2Na_2O_8$), Formaldehyde solution (HCHO), Potassium ferrocyanide (K_4 [Fe (CN) $_6$]) and Polystyrene-*b*-poly (methyl methacrylate) $M_w \sim$ 1,50,000g/mol] and BDH Chemicals [Polystyrene $M_w \sim$ 1,00,000g/mol].

The thin films of conducting polymer composites were fabricated in two phases. In first phase conductive filler was prepared *via* deposition of thin layer of pure copper on the alumina powder using EL deposition approach, whereas in second phase, the thin films of polymer composites were made using the filler prepared in first phase *via* solvent evaporation method.

EL Deposition of Cu onto Al_2O_3

A silk cloth (120 mesh) purchased from local market was used in the form of sachet into which Al_2O_3 particles were packed for EL plating of Cu, eliminating an additional step of filtration after each dipping step. Successful pretreatment was achieved since; the cloth holds Al_2O_3 particles and restricts them to disperse in solution. EL deposition involves following two stages:

Pretreatment of Al_2O_3

Al_2O_3 powder was first dipped in HNO_3 for 2 min to remove the dirt and oil from the surfaces. It was then immersed in acidic micro etching (125 g/L NaCl and 250 mL/L HF solution) for 2 min to make the surface of the particles rough for the proper adhesion of copper particles on the surface. The coarse Al_2O_3 particles were dipped in sensitizing solution (8 g/L $SnSO_4$and 8 mL/L HCl solution) for 2 min. The sensitized Al_2O_3 particles were immersed for 7 min in activation solution prepared (50 mg/L $SnCl_2.2H_2O$, 5 mg/L $PdCl_2$ and 40 mL/L HCl solution) at 35°C to adsorb the catalytic Pd particles. The substrate was washed with deionized water after each step.

Deposition of Cu onto Pretreated Al_2O_3

The copper was deposited on the pretreated Al_2O_3 powder by EL copper deposition technique. The composition of EL plating bath along with required conditions are given in Table I. To analyze the effect of plating time on the deposition of copper, alumina powder was dipped in above solution at different times, i.e., 5, 10, 15 and 30 min. The resultant Cu coated alumina (Cu-Al_2O_3) powder was rinsed in water. The resultant Cu-Al_2O_3 powder was then dried under vacuum at 40°C for 3-4 h and used further to fabricate the conductive polymer composite.

Table I. Composition and Conditions of EL Plating Bath of Copper

Ingredient	Concentration
$CuSO_4.5H_2O$	16 g/L
NaOH	14 g/L
$KNaC_4H_4O_6.4H_2O$	30 g/L
$C_{10}H_{14}N_2Na_2O_8$	20 g/L
HCHO	15 mL/L
K_4 [Fe (CN) $_6$]	25 ppm
pH	12.5
Temperature	40°C

Following Figure 1 shows the comparison of virgin Al_2O_3 and Cu coated Al_2O_3 obtained at its best condition, i.e., with plating time of 30 min.

Fabrication of Conductive Composite Films

The conducting polymer composite was fabricated by dispersing the conducting filler in the polymer solution. The calculated amount of Cu-Al_2O_3 filler (i.e., 3, 6, 9, 12, 15, 18, or 21 wt %) was suspended in the 30 mL THF. The corresponding amount of polymer, i.e., PS-*b*-PMMA or PS was then added to the mixture and was allowed to stirrer for 6 hours. A homogeneously dispersed solution thus obtained was cast in the petri dish placed on a leveled smooth surface. The solvent was evaporated at room temperature. Smooth surfaced, homogeneously distributed films of conducting polymer composites recovered from the petri dish were then dried in vacuum oven till constant weight. The prepared films were subjected to further analysis through various techniques to study their morphological, electrical, thermal and mechanical properties.

Instruments and Methods of Characterization

X-ray Diffraction Analysis. XRD of virgin Al_2O_3, Cu coated Al_2O_3 particles, and of PS-*b*-PMMA/Cu-Al_2O_3 and PS/Cu-Al_2O_3 composites were investigated by using PANalytical X-ray diffractometer (XPERT-PRO) with Cu-Kα X-rays of wavelength (λ) =1.54056 Å. The data was extracted for the 2θ range of 10°

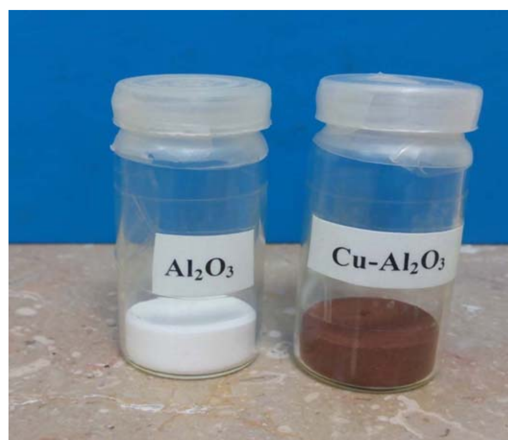

Figure 1. Virgin Al_2O_3 powder and EL coated Cu-Al_2O_3 powder at deposition time of 30 min. [Color figure can be viewed in the online issue, which is available at wileyonlinelibrary.com.]

to 80° with a scan step size of 0.015° and time per step of 0.25 sec, by providing voltage and beam current of 40 kV and 30 mA, respectively. Average crystallite size of Cu coated onto Al_2O_3 particles was calculated by applying the Scherrer equation.

Scanning Electron Microscopy. The surface morphology of Al_2O_3 and Cu-Al_2O_3 particles and fabricated polymer composites were investigated by scanning electron microscopic (SEM) images obtained by Hitachi SU-1500 equipped with secondary electron (SE) detector at an accelerating voltage of 5 kV.

Energy Dispersive Spectrometry Analysis. Atomic % of elements in Cu-Al_2O_3 particles and fabricated polymer composites were investigated by JSM6490LV (JEOL) microscope equipped with QUANTAX EDS XFlash detector 4010 (Bruker) for EDX analysis at an accelerating voltage of 20 kV.

Volume Resistivity Measurements. The volume resistivity (Ω.cm) of composite films was measured by 4-probe method at room temperature using Insulation Tester (NF2511) with tungsten carbide electrodes by providing a direct current field of 500V along the direction of film thickness. Since, electrical conductivity (S/cm) is the inverse of volume resistivity (1/Ω.cm), the inverse of volume resistivity values was taken to obtain electrical conductivity of the prepared composites.

Mechanical Studies. Mechanical properties of composites were analyzed to calculate Young's modulus (MPa), tensile strength (MPa) and % elongation at break. Mechanical analysis was done according to American Society for Testing and Materials (ASTM) D638-02 and D638-03. A sample having thickness of 0.8-1.0 mm and with dimensions 6 × 70 mm (width × gauge length) was subjected to Instron Tester (4600 UK) at test temperature of 20 ± 2°C.

Thermal Studies. Thermogravimetric analysis (TGA) was carried out between 44 and 580°C at 10°C/min with constant N_2 environment using Perkin Elmer TGA-7 taking 2 mg of sample. The rate of flowing N_2 was 20 mL/min. Thermal analytical results were recorded in non-isothermal conditions. Differential Scanning Calorimetry (DSC) of the prepared composites was also analyzed between 40 and 500°C at 10°C/min by using DSC 404-NETZSCH instrument.

RESULTS AND DISCUSSION

X-ray Diffraction Analysis of Virgin and Cu Coated Al_2O_3 Powder

In order to analyze the effect of plating time on the crystallite size of plated Cu, XRD analysis of virgin Al_2O_3 and Cu plated Al_2O_3 was carried out by varying plating time for 5, 15, and 30 min, as shown in Figure 2(a–d). Crystallite size of plated Cu was calculated by applying the Scherrer's equation, expressed in eq. (1) as follows[18]:

$$D = \frac{K\lambda}{\beta \cos\theta} \tag{1}$$

Where, D corresponds to crystallite size (nm), λ is the X-ray wavelength (nm), K is Scherrer's constant usually taken as 0.9, β is angular width expressed in radians, and θ is the Bragg's angle (deg).

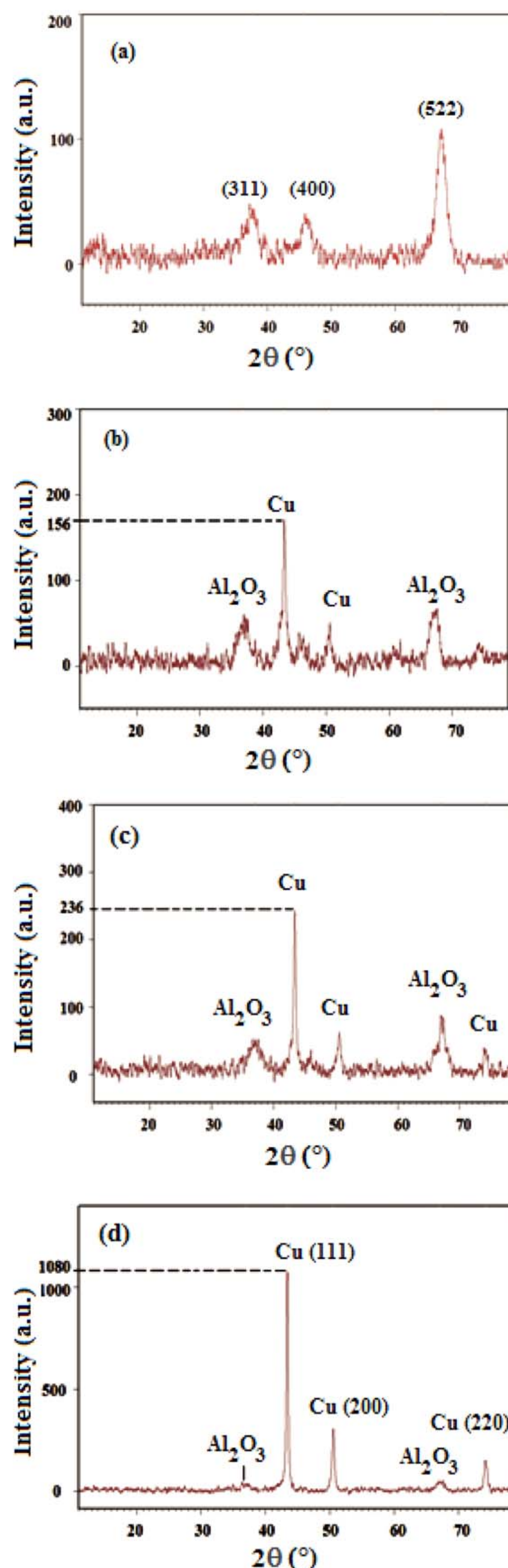

Figure 2. XRD patterns of (a) virgin Al_2O_3 powder; (b) Cu-Al_2O_3 powder at deposition time 5 min; (c) 15 min and (d) 30 min. [Color figure can be viewed in the online issue, which is available at wileyonlinelibrary.com.]

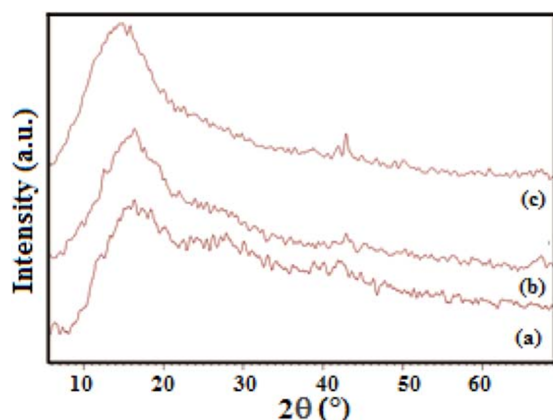

Figure 3. XRD patterns of (a) neat PS-b-PMMA; (b) PS-b-PMMA with 3 wt % Cu-Al_2O_3 and (c) PS-b-PMMA with 21 wt % Cu-Al_2O_3. [Color figure can be viewed in the online issue, which is available at wileyonlinelibrary.com.]

Figure 2(a) depicts the XRD pattern of virgin Al_2O_3 powder. Three peaks at 2θ values of 37.5726, 45.7703 and 67.2631 deg correspond to Al_2O_3 phase. Two 2θ peaks at 43.326 and 50.4858 deg emerged after plating time of 5 min with average crystallite size of 16.728 nm (Figure 2b). After plating time of 15 min, average crystallite size of deposited Cu increased up to 20.05 nm (Figure 2c) which further increased to 26.116 nm after plating time of 30 min (Figure 2d). The disturbance observed in the peaks corresponding to Al_2O_3 phase is due to the change in the nature of original Al_2O_3 after the deposition of Cu.[19–21] Comparing the three Cu-Al_2O_3 XRD patterns it is observed that the strongest peak of Cu at $2\theta = 43$ deg narrowed and showed uniform increase in peak intensity due to increased Cu crystallite size with increased plating time. Thus, optimized plating time of 30 min was optimized for further preparation and characterization of EL deposited Cu-Al_2O_3 powder. Similar XRD pattern was reported in the literature[22,23] where strongest peak of EL deposited Cu appeared at $2\theta = 43$ deg.

XRD pattern of Cu coated Al_2O_3 did not reveal any peak related to Pd. Similar behavior has been shown by the XRD analysis of Cu coated Al_2O_3 reported in the literature[19,21] where only Cu^0 and Al_2O_3 diffraction peaks were observed. This might be attributed due to the fact that the Pd^0, deposited on Al_2O_3 as nucleating site for Cu^0, is minute in concentration and might get influenced by the relatively large crystallite size of Cu^0.

X-ray Diffraction Analysis of Block Copolymer and Homopolymer Composites

In order to investigate the effect of Cu-Al_2O_3 filler in PS-*b*-PMMA and PS host polymers, X-ray diffraction patterns of neat PS-*b*-PMMA and PS; PS-*b*-PMMA and PS with 3 wt %; and 21 wt % Cu-Al_2O_3 were recorded. As shown in Figure 3(a), the XRD pattern depicted a broad noncrystalline peak (10–30 deg) of neat PS-*b*-PMMA. This peak is the characteristic of pure PS-*b*-PMMA and is also observed in the literature.[24] With the incorporation of 3 wt % Cu-Al_2O_3, a small peak appeared at $2\theta = 42.9$ deg (Figure 3b) which increased its intensity with the increase of Cu-Al_2O_3 content upto 21 wt % (Figure 3c). Also it seemed that that the intensity of the broad peak of neat PMMA got increased with filler inclusion. This increase in the peak intensities might be attributed to the increase of the crystalline region of Cu-Al_2O_3 (Table II).

Table II. intensity of X-ray Diffraction Peaks Observed in XRD Analysis of PS-*b*-PMMA and PS Composites as a Function of Cu-Al_2O_3 Content

Composite Type	Cu-Al_2O_3 (wt %)	Diffraction angle (2θ)	Intensity at diffraction peaks (counts/sec)
PS-*b*-PMMA/Cu-Al_2O_3	0 (neat polymer)	10–30	64–148
	3	10–30	175–288
		42.9	132
	21	10–30	186–379
		42.9	164
PS/Cu-Al_2O_3	0 (neat polymer)	10–19.7	232–317
	3	10–19.7	42–109
		42.9	186
		66.7	92
	21	10–19.7	169–506
		42.9	288
		50.3	165

Similar XRD pattern was observed in case of neat PS (Figure 4a) where a broad peak at 2θ (10-19.7 deg) indicate an amorphous structure.[25] Inclusion of 3 wt % Cu-Al_2O_3 resulted in the appearance of two peaks at $2\theta = 42.9$ deg and 66.7 deg (Figure 4b). Further incorporation of filler depicted two peaks at $2\theta = 42.9$ deg with increased intensity compared to 3 wt % filler loading and at $2\theta = 50.3$ deg (Figure 4c). A slight shift of PS peak with increased intensity was also observed at 21 wt % filler content which might be attributed to the effect of crystalline nature of Cu-Al_2O_3. The significant increase of the intensities in both types of polymers

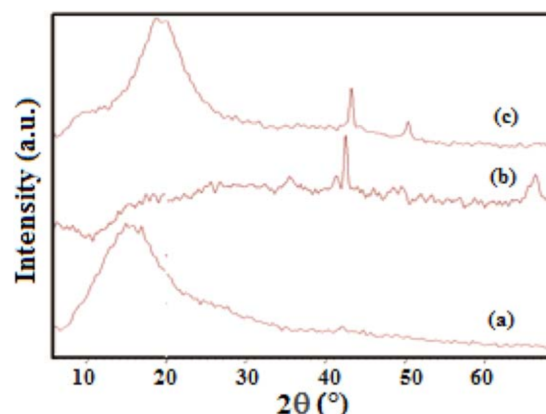

Figure 4. XRD patterns of (a) neat PS; (b) PS with 3 wt % Cu-Al_2O_3 and (c) PS with 21 wt % Cu-Al_2O_3. [Color figure can be viewed in the online issue, which is available at wileyonlinelibrary.com.]

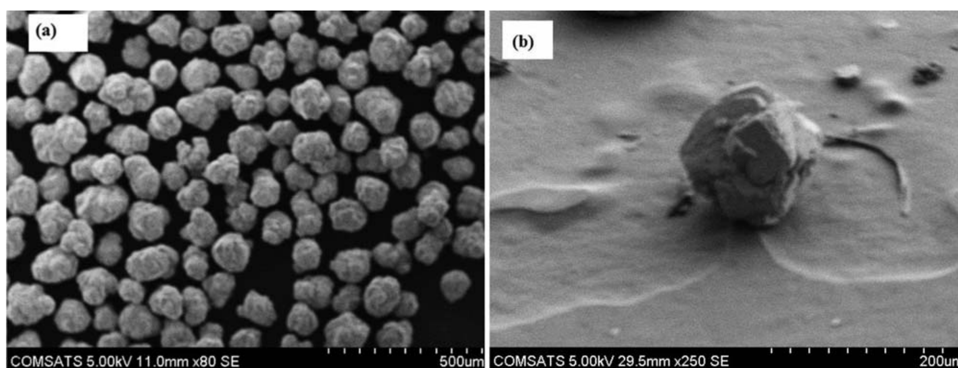

Figure 5. SEM micrographs of (a) virgin Al_2O_3 powder and (b) virgin Al_2O_3 particle.

(Figures 3 and 4) show the increase of the crystallinity in the polymers (Table II).

Peak at $2\theta = 42.9$ deg found in the both types of composites, is a characteristic peak of Cu (111) also observed in XRD pattern of Cu coated Al_2O_3 powder (Figure 2b–d).

Morphological Studies of Virgin and Cu Coated Al_2O_3 Powder by Scanning Electron Microscopy (SEM)

Al_2O_3 particles exhibited fine dispersion as compared to Cu-Al_2O_3 with little agglomeration seen between few particles. Analyzing the shape of the particles revealed that they are almost spherical in shape and appeared smoother as compared to Cu-Al_2O_3, as evident in Figure 5(a,b), respectively.

As given in Figure 6(a), surface analysis of Cu-Al_2O_3 particles revealed uniform deposition of Cu over Al_2O_3 particles and it seems that no Al_2O_3 particle remained uncoated or poorly coated, confirming the uniform interaction of EL plating bath with all the particles of Al_2O_3. Similar to virgin Al_2O_3, Cu-Al_2O_3 particles also exhibited spherical appearance, explaining uniform deposition. A fine scale roughness of Cu observed over the entire surface of Al_2O_3 is a characteristic of metallic film deposition.[19]

As shown in Figure 6(a), Cu coated Al_2O_3 powder exhibits aggregation of particles not seen in case of virgin Al_2O_3 powder. This might be attributed to the weak interactions existing between Cu coated particles.[26]

Similar results have been reported in the literature regarding the morphology of EL plated Cu onto Al_2O_3 powder. Silvain and coworkers,[27] deposited Cu onto sub micron sized Al_2O_3 particles by using EL coating method. SEM analysis revealed uniform and fine coating of metallic Cu and increase in average particle size of Al_2O_3 particles after Cu deposition.

Wang and coworkers,[21] also conducted EL deposition of Cu onto Al_2O_3 powder. The reported SEM micrographs also revealed uniform deposition of Cu over the entire surface of Al_2O_3 particles at an optimized time of 30 min. This also confirms that the plating time of 30 min selected for the Cu deposition of currently prepared Cu-Al_2O_3 filler is ideal condition to plate Cu onto Al_2O_3.

To compare the morphological properties of currently prepared Cu-Al_2O_3 powder with the literature reporting the EL deposition of Cu on Al_2O_3 powder, following Figure 7 is taken from the work of Wang and coworkers.[21]

The fine scale roughness due to metallic Cu coating and aggregation of Cu-Al_2O_3 particles depicted in the reported[21] Figure 7, is comparable to and almost similar to the morphology of Cu-Al_2O_3 particles of the currently prepared Cu-Al_2O_3 powder shown in Figure 6(a).

Morphological Studies of Block Copolymer and Homopolymer Composites by Scanning Electron Microscopy (SEM)

SEM images of neat PS-*b*-PMMA and PS-*b*-PMMA with 3, 9, 15 and 21 wt % Cu-Al_2O_3 loadings are shown in Figure 8(a–e),

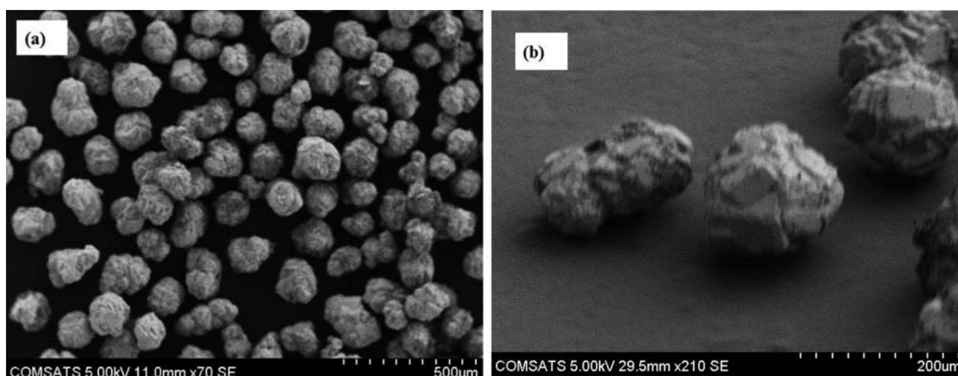

Figure 6. SEM micrographs of (a) Cu coated Al_2O_3 powder and (b) Cu coated Al_2O_3 particle.

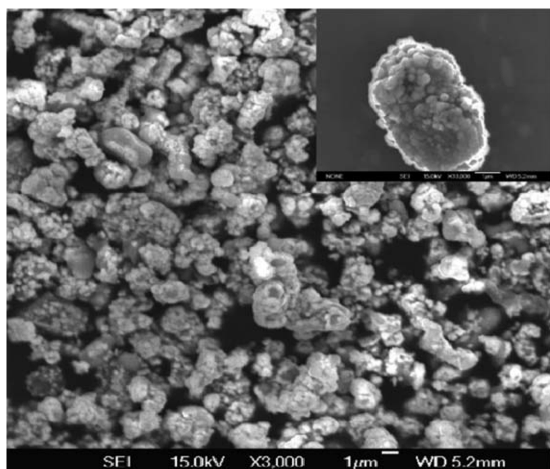

Figure 7. Reported SEM micrograph of EL coated Cu onto Al_2O_3 powder at plating time 30 min by Wang and coworkers.[2]

respectively. SEM micrographs of neat PS and PS with 3, 9, 15 and 21 wt % Cu-Al_2O_3 loadings are also shown in Figure 9(a–e), respectively.

Formation of conductive network depends upon the interaction between conductive filler particles.[20] With increased filler content up to 9 wt %, though, filler particles are dispersed within the matrix, yet no connectivity among the conductive filler particles has developed. This indicates that for both types of matrices, 9 wt % content of Cu-Al_2O_3 is not sufficient to create well developed particle to particle interaction.[28] The increased filler loading up to 15 wt % revealed a pronounced effect on the fracture surface of PS-*b*-PMMA and PS based composites. Significant increase in bright phases of the two composites corresponds to increased loadings of metallic Cu coated alumina particles. Filler particles are completely embedded within the matrix and no phase separation is seen predicting good filler–polymer interaction. Increasing Cu-Al_2O_3 content up to 15 wt %

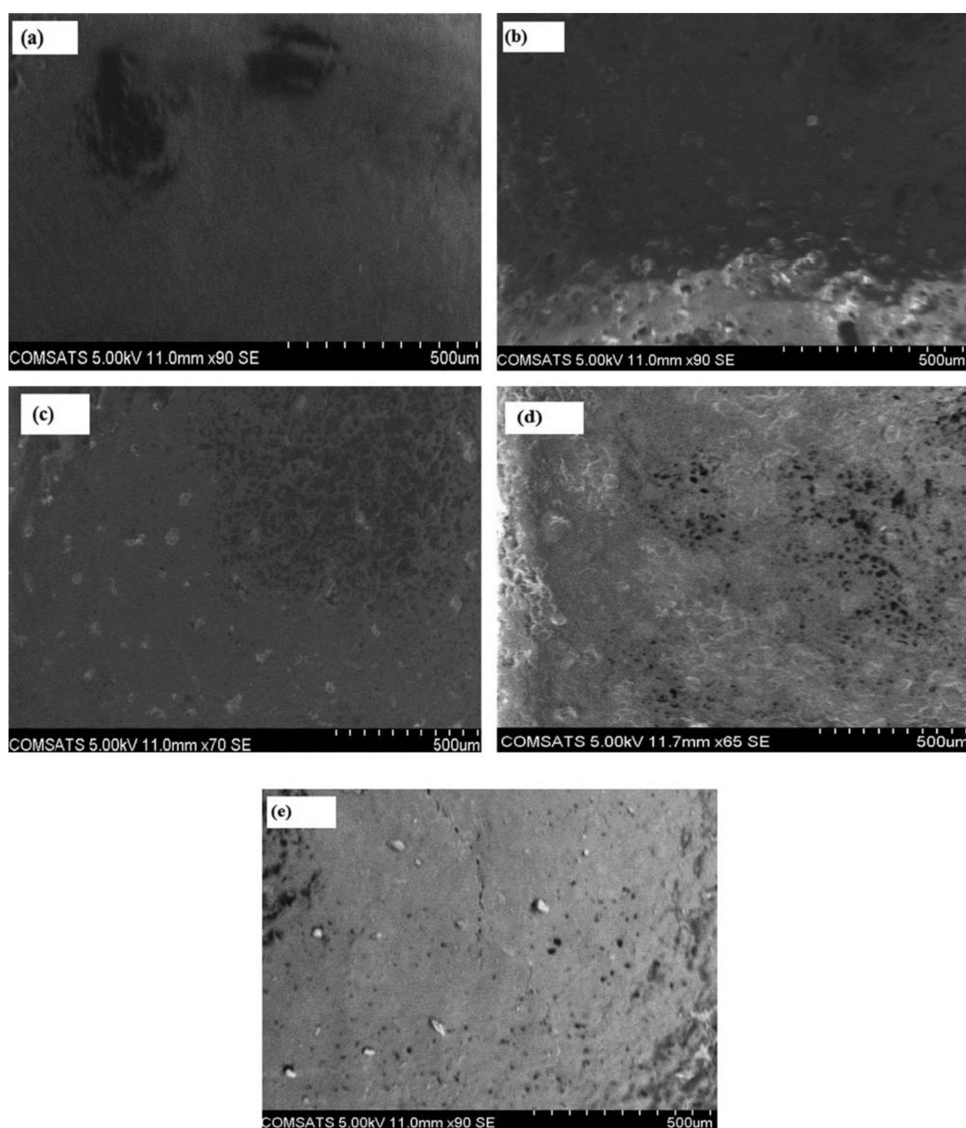

Figure 8. SEM micrographs of (a) Neat PS-*b*-PMMA; (b) PS-*b*-PMMA with 3 wt % Cu-Al_2O_3; (c) PS-*b*-PMMA with 9 wt %; (d) PS-*b*-PMMA with 15 wt % and (e) PS-*b*-PMMA with 21 wt % Cu-Al_2O_3.

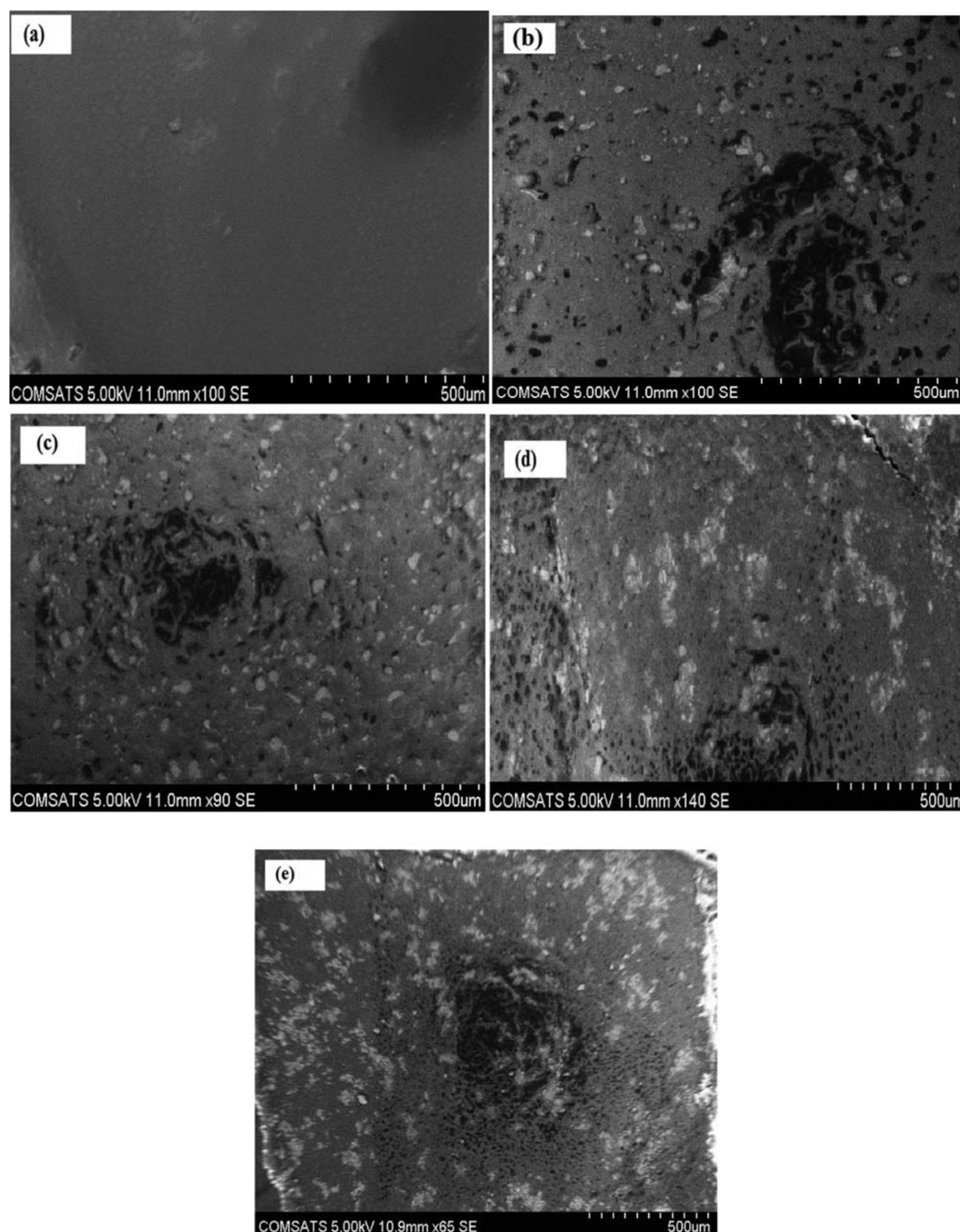

Figure 9. SEM micrographs of (a) Neat PS; (b) PS with 3 wt % Cu-Al_2O_3; (c) PS with 9 wt %; (d) PS with 15 wt % and (e) PS with 21 wt % Cu-Al_2O_3.

showed initiation of particle-to-particle connectivity in both composite films which is more visible in case of PS-PMMA composites with 15 wt % filler. These clusters distinctly grew throughout the matrices when the filler concentration was further increased to 21 wt % which also improved the bright phases of the composites with well developed particle–particle connectivity. An obvious transition from particle–polymer contact to well developed particle–particle contact is seen. Few of the Cu-Al_2O_3 particles protrude out of the matrices which indicate that maximum loading capacity of polymer matrices is attained. Appearance of micro crack in PS-PMMA composite with 21 wt % filler, not seen in case of PS composite with similar concentration, explains the slightly higher brittle behavior of PS–PMMA composite imparted by PMMA block present in PS–PPMA.

Table III. Atomic % of Elements in Cu-Al_2O_3 Powder

Element type	Atomic % of Elements
Cu	65.08
Al	31.25
Pd	3.67
Total	100

Energy Dispersive Spectrometry Analysis of Cu-Al_2O_3 Filler and Block Copolymer and Homopolymer Composites

Energy dispersive spectrometry (EDX) analysis was done to analyze the elemental composition of the Cu coated Al_2O_3 filler. As

Table IV. Atomic % of Elements in PS-*b*-PMMA/Cu-Al_2O_3 and PS/Cu-Al_2O_3 Composites

Composite Type	Cu-Al_2O_3 (wt %)	Atomic % of elements				
		C	O	Al	Cu	Pd
PS-*b*-PMMA/ Cu-Al_2O_3	3	78.29	21.64	0.05	0.02	0.00
	15	78.08	21.79	0.05	0.07	0.01
	21	78.89	20.82	0.07	0.20	0.02
PS/Cu-Al_2O_3	3	78.03	21.88	0.07	0.02	0.00
	15	78.08	21.79	0.05	0.07	0.01
	21	78.70	20.98	0.11	0.20	0.01

shown in Table III, three elements Al, Cu, and Pd were detected, Cu being major in composition (65.08%) followed by Al (31.25%) and Pd (3.67%). Presence of Cu in such high concentration also confirms the effective coating of Al_2O_3. The presence of Pd is due to the use of $PdCl_2$ as an activator during the EL coating of Cu.

Elemental composition and atomic % of respective elements present in PS-*b*-PMMA and PS composites have also been studied *via* EDX. Five different elements C, O, Al, Cu, and Pd have been analyzed and their atomic % is presented in Table IV. Atomic % of Al, Cu, and Pd increased with Cu-Al_2O_3 filler wt % in both types of composites. Out of the five studied elements, Pd is detected in least atomic % which might be attributed to the lowest concentration of $PdCl_2$ used during EL coating process for surface activator of Al_2O_3.

Volume Resistivity/Electrical Conductivity Analysis of Block Copolymer and Homopolymer Composites

The volume resistivity of PS-*b*-PMMA and PS matrix composites were examined as a function Cu-Al_2O_3 filler loadings, i.e., 0, 3, 6, 9,12,15,18 and 21 wt %. Table V depicts the volume resistivity (Ω.cm) and electrical conductivity (S/cm) values of PS-*b*-PMMA and PS matrix composites with increased Cu-Al_2O_3 filler loading. Since, volume resistivity is the inverse of conductivity, the drop-off in the values of volume resistivity is

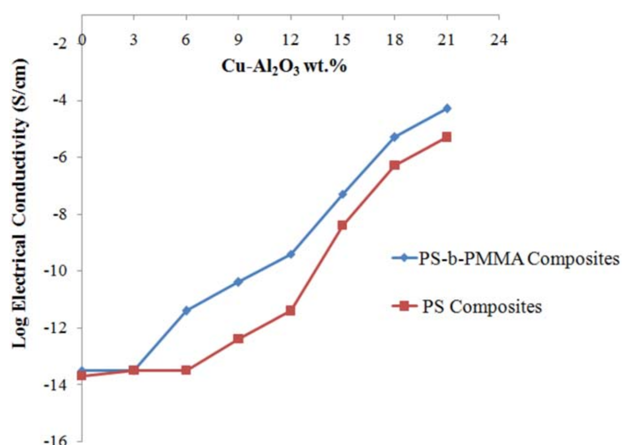

Figure 10. Effect of Cu-Al_2O_3 filler on electrical conductivity of PS-*b*-PMMA and PS composites. [Color figure can be viewed in the online issue, which is available at wileyonlinelibrary.com.]

inversely proportional to the increase in the electrical conductivity of the prepared composites. The log values of electrical conductivity (S/cm) of respective composites are shown in Figure 10.

Neat PS-*b*-PMMA and PS films with 0 wt % Cu-Al_2O_3 loading depicted electrical conductivity of 3.33×10^{-14} S/cm and 2.0×10^{-14} S/cm, respectively, confirming the insulating behavior of selected matrices. The increment in conductivity values started with the incorporation of lowest filler content of 3 wt %, and a significant increase in conductivity up to 4.54×10^{-8} S/cm for PS-*b*-PMMA and 4.35×10^{-9} S/cm for PS is achieved till 15 wt % but still these values lie in the insulating region. This might be attributed to the low filler content which results in sufficiently large distance as such they disperse more homogenously throughout the matrix resulting in lesser particle-to-particle interaction.[29] Incorporation of 21 wt % Cu-Al_2O_3 loading revealed maximum increase in conductivity of 5.55×10^{-5} S/cm for PS-*b*-PMMA and 5.0×10^{-6} S/cm for PS composites. This increase confirms the attainment of semi-conducting properties in both composites. It is known that the conductive behavior of a polymer composite depends upon the proper particle–particle contact. Thus, transmission of electrons from one

Table V. Volume Resistivity and Electrical Conductivity Values of PS-*b*-PMMA and PS Composites as a Function of Cu-Al_2O_3 Content

Cu-Al_2O_3 (wt %)	Electrical properties of PS-*b*-PMMA composites		Electrical properties of PS composites	
	Volume resistivity (Ω.cm)	Conductivity (S/cm)	Volume resistivity (Ω.cm)	Conductivity (S/cm)
0	3.0×10^{13}	3.33×10^{-14}	5.0×10^{13}	2.0×10^{-14}
3	2.7×10^{13}	3.704×10^{-14}	3.1×10^{13}	3.23×10^{-14}
6	2.6×10^{11}	3.85×10^{-12}	2.9×10^{12}	3.45×10^{-13}
9	2.4×10^{10}	4.16×10^{-11}	2.7×10^{12}	3.70×10^{-13}
12	2.3×10^{9}	4.35×10^{-10}	2.6×10^{11}	3.85×10^{-12}
15	2.2×10^{7}	4.54×10^{-8}	2.3×10^{8}	4.35×10^{-9}
18	2.0×10^{5}	5.0×10^{-6}	2.11×10^{6}	4.74×10^{-7}
21	1.8×10^{4}	5.55×10^{-5}	2.0×10^{5}	5.0×10^{-6}

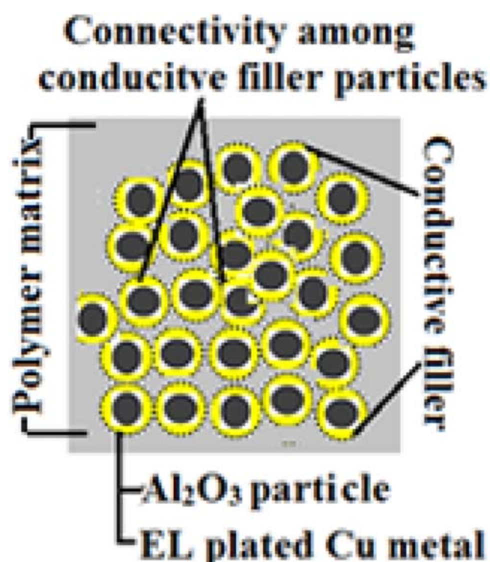

Figure 11. Schematic representation of interaction among PS-*b*-PMMA or PS polymer matrix and prepared Cu-Al_2O_3 conductive filler. [Color figure can be viewed in the online issue, which is available at wileyonlinelibrary.com.]

particle to the other that are dispersed throughout the matrix takes place only if the particles are geometrically connected to each other, forming a network. This increment in conductivity might be attributed to the formation of conducting networks at 21 wt % Cu-Al_2O_3 loading which facilitated electron transfer throughout the PS-*b*-PMMA and PS matrix[30] which can be illustrated as shown in Figure 11.

Presently prepared composites exhibit better electrical conductivity properties along with the ease of preparation and cost-effectiveness as compared to previously reported conductive composites,[31] where waterborne polyurethane/functionalized graphene sheets nanocomposites were prepared by casting from a colloidal dispersion.

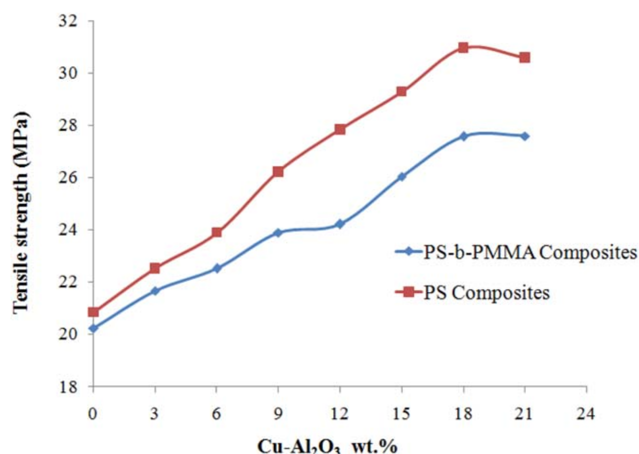

Figure 13. Effect of Cu-Al_2O_3 filler on Tensile Strength of PS-*b*-PMMA and PS composites. [Color figure can be viewed in the online issue, which is available at wileyonlinelibrary.com.]

Mechanical Analysis of Block Copolymer and Homopolymer Composites

Young's Modulus. According to the results, Young's modulus of PS-*b*-PMMA composites was found in the range of 680-1122 MPa, as given in Figure 12. Incorporation of 3 wt % Cu-Al_2O_3 filler increased the Young's modulus up to 758 MPa. When the filler content was gradually increased to 21 wt %, the Cu-$Al_2O_{3/}$PS–PMMA composite exhibited highest Young's modulus of 1122 MPa, significantly higher than that of neat PS-*b*-PMMA (680 MPa). Similar behavior was observed in case of Cu-$Al_2O_{3/}$PS composites. A significant increase in Young's modulus from 680.12 MPa to 1053.9 MPa was achieved with the incorporation of 21 wt % of Cu-Al_2O_3 into the neat PS. Since, ceramics possess higher modulus than that of the neat polymers, increase in Young's modulus is observed due to the rigidity associated with Al_2O_3 which may provide stiffness to both PS-*b*-PMMA and PS matrices.[32]

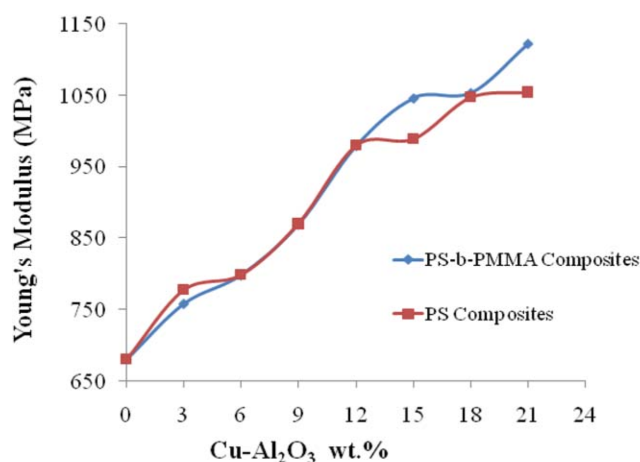

Figure 12. Effect of Cu-Al_2O_3 filler on Young's Modulus of PS-*b*-PMMA and PS composites. [Color figure can be viewed in the online issue, which is available at wileyonlinelibrary.com.]

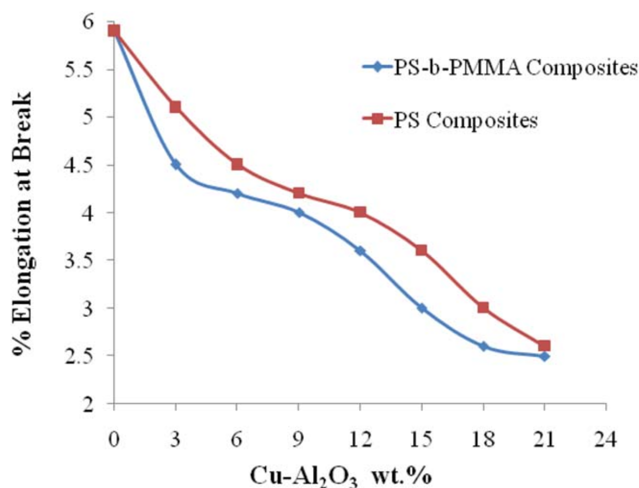

Figure 14. Effect of Cu-Al_2O_3 filler on % Elongation at Break of PS-*b*-PMMA and PS composites. [Color figure can be viewed in the online issue, which is available at wileyonlinelibrary.com.]

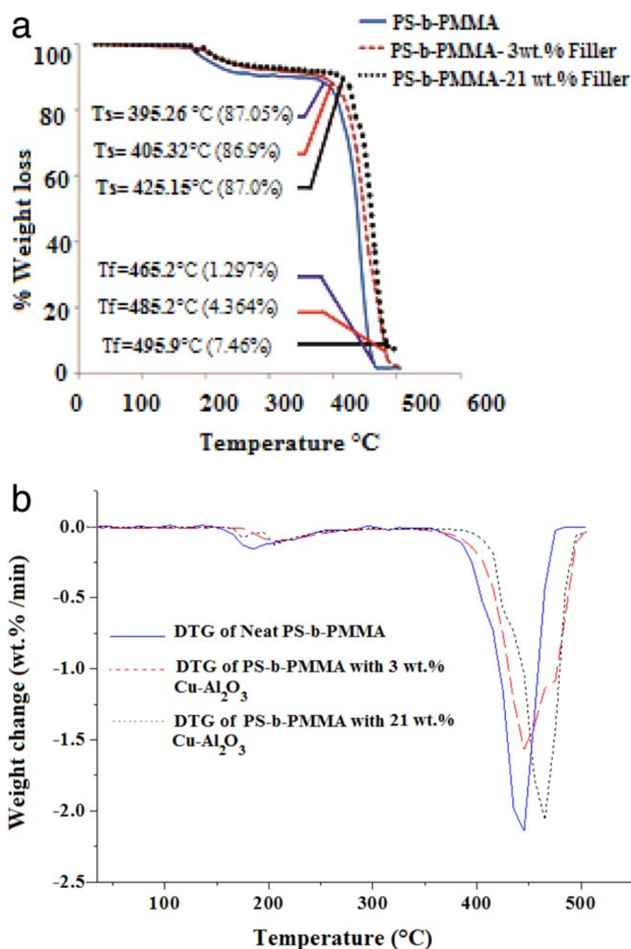

Figure 15. (a) TG thermograms of Neat PS-*b*-PMMA; PS-*b*-PMMA with 3 wt % Cu-Al_2O_3 and PS-*b*-PMMA with 21 wt % Cu-Al_2O_3. (b) DTG of Neat PS-*b*-PMMA; PS-*b*-PMMA with 3 wt % Cu-Al_2O_3 and PS-*b*-PMMA with 21 wt % Cu-Al_2O_3. [Color figure can be viewed in the online issue, which is available at wileyonlinelibrary.com.]

Tensile Strength. A material's strength is related with its ability to sustain the maximum tensile stress before its breakage or failure. In case of composites, it is the effective transfer of stress between matrix and the reinforcements.

Figure 13 explains influence of Cu-Al_2O_3 content on the tensile strength of the PS-*b*-PMMA and PS composites. In the composite films prepared by using PS-*b*-PMMA, an increase in tensile strength with increased filler content was observed in both types of polymer composites. In case of neat PS-*b*-PMMA and its composites, tensile strength increased from 20.229 MPa to 27.998 MPa while that of neat PS and its composites exhibited increment from 20.836 MPa to 30.585 MPa. This exhibits good compatibility between Cu-Al_2O_3 particles and polymer matrices and ensures the effective transfer of stress from the matrix to filler phase which is a characteristic of composites with enhanced tensile properties. If compared, PS-*b*-PMMA composites showed lesser increment in tensile properties than PS composites due to the presence of hard polar PMMA segment in the polystyrene (PS-*b*-PMMA) which has tightly bound the chains of polymer and has reduced filler loading capacity of PS-*b*-PMMA.[33,34] Comparing the tensile strength of the currently prepared composites with the literature,[31] results revealed that PS-*b*-PMMA and PS composites offered good strength and stability.

% Elongation at Break. A decreasing trend in % elongation at break is observed when the Cu-Al_2O_3 was loaded as filler in both the polymer matrices used. As shown in Figure 14, neat PS-*b*-PMMA and PS exhibited 5.9% elongation at break which reduced to 2.5% in case of PS-*b*-PMMA and 2.6% in case of PS matrix when filler loading was increased to 21 wt %. It is known that polymers are ductile in nature while ceramics possess brittle behavior.[35] Addition of rigid Cu-Al_2O_3 filler into the PS-*b*-PMMA and PS matrices monotonically increased the brittleness of the composites and transformation from the ductile behavior of PS-*b*-PMMA and PS towards the brittle behavior of Cu-Al_2O_3/PS-*b*-PMMA and Cu-Al_2O_3/PS composites was observed.[36]

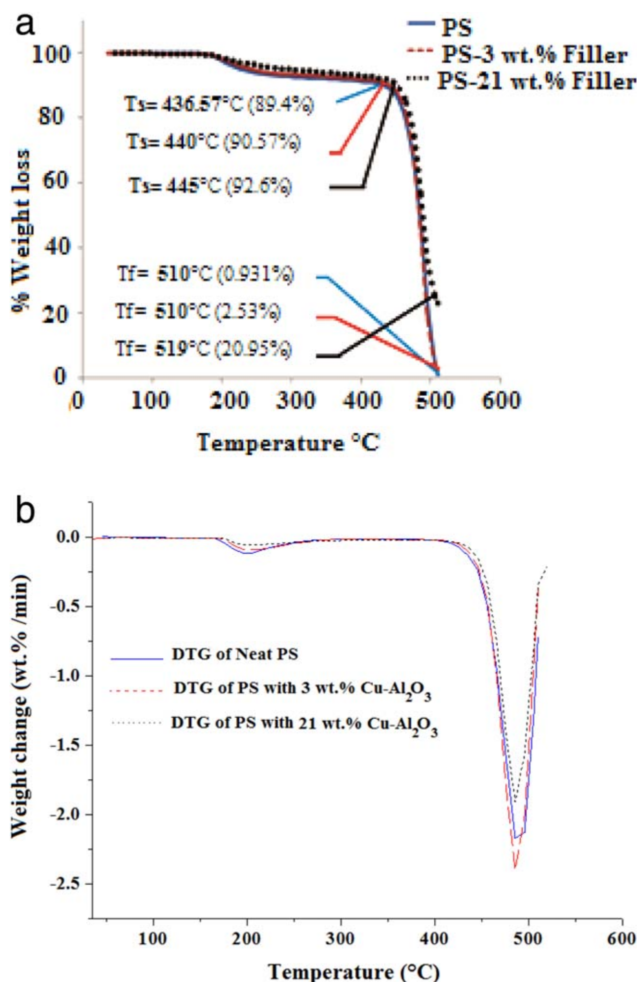

Figure 16. (a) TG thermograms of Neat PS; PS with 3 wt % Cu-Al_2O_3 and PS with 21 wt % Cu-Al_2O_3. (b) DTG of Neat PS; PS with 3 wt % Cu-Al_2O_3 and PS with 21 wt % Cu-Al_2O_3. [Color figure can be viewed in the online issue, which is available at wileyonlinelibrary.com.]

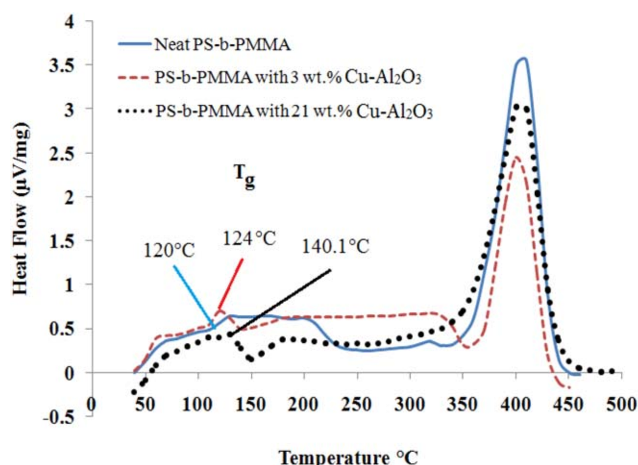

Figure 17. DSC thermograms of Neat PS-*b*-PMMA; PS-*b*-PMMA with 3 wt % Cu-Al_2O_3 and PS-*b*-PMMA with 21 wt % Cu-Al_2O_3. [Color figure can be viewed in the online issue, which is available at wileyonlinelibrary.com.]

Thermal Studies of Block Copolymer and Homopolymer Composites

Thermogravimetric Analysis (TGA). Previous studies have shown that a polymer matrix reinforced with inorganic filler exhibited improved thermal stability along with enhanced resistance to thermal degradation.[37]

TGA of neat PS-*b*-PMMA, PS-*b*-PMMA/Cu-Al_2O_3 composites and their derivative curves are shown in Figure 15(a,b), respectively. The TG curve of neat PS-*b*-PMMA, revealed two steps decomposition. The on-set degradation temperature of neat PS-*b*-PMMA corresponds to 180°C with slight decrease in weight % of 0.6345%. Uptill 395.26°C, the polymer remained almost stable with 12% weight loss. Thus, 395.26°C temperature corresponds to maximum stability temperature (T_s) after which an abrupt weight loss was observed which continued till 465.61°C which is the final degradation temperature (T_f) with % residue of 2.19%. With the inclusion of 3 wt % Cu-Al_2O_3 [Figure 15(a)], T_s increased from 395.26°C (neat PS-*b*-PMMA) to 405.32°C while no significant change was observed in on-set degradation temperature which showed an increase of 1°C compared to neat polymer. T_f was also increased from 465.61°C to 485.24°C due the presence of ceramic filler with 3.08% residue. Incorporation of 21 wt % filler increased T_s of up to 30°C (425.12°C) as compared to neat polymer while on-set degradation temperature remained at 181°C . The % residue of 7.46% observed at T_f of 495.98°C corresponds to the presence of Cu-Al_2O_3 filler which has higher thermal stability as compared to polymer matrix. Two-step degradation profiles were also observed in the derivative curves of neat PS-*b*-PMMA and its composites, confirmed from the presence of two distinct peaks shown in Figure 15(b). In case of neat PS and PS/Cu-Al_2O_3 composites [Figure 16(a)] increased filler loading also increased thermal stability of the resultant composites. Compared to PS-*b*-PMMA composites, incorporation of filler into PS exhibited a significant increase in on-set degradation temperature from 179°C, observed in case of neat PS, to 192°C and then 250°C, observed with inclusion of 3 wt % and 21 wt % Cu-Al_2O_3 filler, respectively. The derivative curves of neat PS and respective composites also exhibited two-step thermal degradation that can be seen in Figure 16(b). Upon heating the long chains of polymer broke down into small fragments. These small fragments might interact with Cu-Al_2O_3 particles and get trapped into filler particles and are difficult to be decomposed further, aiding in increased thermal stability of the PS-*b*-PMMA and PS composites.[34]

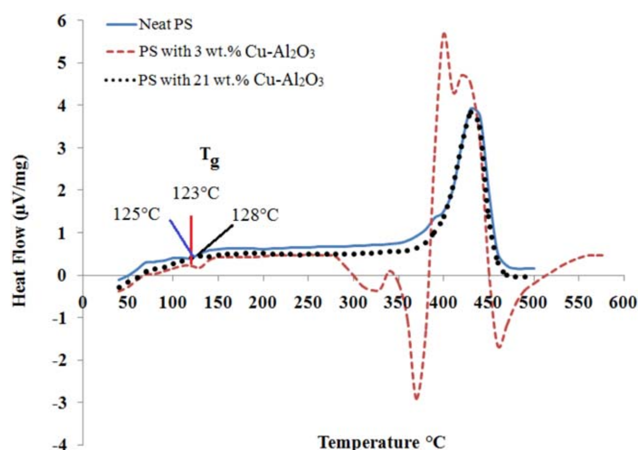

Figure 18. DSC thermograms of Neat PS; PS with 3 wt % Cu-Al_2O_3 and PS with 21 wt % Cu-Al_2O_3. [Color figure can be viewed in the online issue, which is available at wileyonlinelibrary.com.]

Differential Scanning Calorimetry (DSC). In case of PS-*b*-PMMA composites, DSC thermograms revealed difference in glass transition temperature (T_g) observed as a function of filler loading. Neat PS-*b*-PMMA exhibited T_g of 120°C, as shown in Figure 17. Incorporation of 3 wt % Cu-Al_2O_3 depicted increase in T_g up to 124°C. This increment became pronounced with the inclusion of 21 wt % Cu-Al_2O_3 loading exhibiting T_g up to 140°C. It is known that polar polymers show more affiliation towards conducting fillers.[38] The interaction of metal (Cu deposited on Al_2O_3) with the PMMA block might be responsible for this shift of T_g towards higher side. It is known that at T_g, polymer chains start to move. The results showed that the incorporation of 21 wt % of Cu-Al_2O_3 into PS-*b*-PMMA matrix increases its T_g as chains of PS-*b*-PMMA were strongly adhering with the Cu-Al_2O_3 particles, which prevented the segmental movement of chains.[39]

DSC thermogram of neat PS exhibited T_g of 125°C, as exhibited in Figure 18. The increased filler loading from 3 wt % to 21 wt % produced no significant change in the value of T_g which remained at 128°C. These results suggest that due to the non-polar behavior of PS only physical interaction persists between filler and PS matrix.[40]

CONCLUSIONS

Novel electrically conductive Cu-Al_2O_3/PS-*b*-PMMA and Cu-Al_2O_3/PS composites were successfully fabricated using EL deposition as a new technique for conducting composite preparation. XRD pattern confirmed the deposition of metallic Cu onto Al_2O_3 at an optimized time of 26.116 nm. Significant change in XRD patterns of neat PS-*b*-PMMA and PS was observed with inclusion of Cu-Al_2O_3. SEM micrographs of both types of composite films revealed improved particle-particle interaction with gradual increment in filler content. EDX analysis also confirmed the presence of Cu in both filler and polymer

composites along with other elements. Incorporation of Cu-Al_2O_3 into polymer matrices significantly increased their electrical conductivity values with PS-*b*-PMMA composites showing semi-conductive behavior at 21 wt % filler loading compared to PS composites with similar loading. Increased filler loading imparted rigidity which resulted in increased Young's Modulus and decreased % elongation at break of the two composites. Both types of composites revealed increased tensile strength and thus improved mechanical stability with increased Cu-Al_2O_3 content. TG results revealed improved thermal stability in both composites with increased filler loading while DTG curves confirmed two-step degradation behavior of the composites. DSC results confirmed shift of T_g towards higher values for PS-*b*-PMMA based composites as a function of filler loading while T_g of PS composites showed no pronounced change. Considering these results currently prepared composites may find their futuristic application as semiconductors in the electronic industry and are likely to fulfill the requirements of microelectronic packaging, anti-static coatings for electronic devices, etc., and thus, may improve the shelf life of electronic products.

ACKNOWLEDGMENTS

The authors are grateful to Prof. Dr. Arshad S. Bhatti at Nano Labs of COMSATS Institute of Information Technology, Islamabad for the valuable assistance in the SEM analysis.

REFERENCES

1. Li, J. X.; Wu, J.; Chan, C. M. *Polymer* **2000**, *41*, 6935.
2. Reynaud, E.; Jouen, T.; Gauthier, C.; Vigier, G.; Varlet, J. *Polymer* **2001**, *42*, 8759.
3. Tongxiang, L.; Wenli, G.; Yinghui, Y.; Chunhe, T. *Int. J. Adhes. Adhes.* **2007**, *28*, 55.
4. Pang, X.; Zhitomirsky, I.; Niewczas, M. *Surf. Coat. Technol.* **2005**, *195*, 138.
5. Reina, A.; Jia, X.; Ho, J.; Nezich, D.; Son, H.; Bulovic, V.; Dresselhaus, M. S.; Kong, J. *Nano Lett.* **2008**, *99*, 30.
6. Cuna, A.; Noguera, A.; Saucedo, E.; Fornaro, L. *Cryst. Res. Technol.* **2004**, *39*, 912.
7. Reddy, K. R.; Lee, K. P.; Gopalan, A. I. *Colloids Surf. A* **2008**, *320*, 49.
8. Reddy, K. R.; Jeong, H. M.; Lee, Y.; Raghu, A. V. *J. Polym. Sci., Part A: Polym. Chem.* **2010**, *48*, 1477.
9. Feng, Z. Q.; Wu, J.; Cho, W.; Leach, M. K.; Franz, E. W.; Naim, Y. I.; Gu, Z.; Corey, J. M.; Martin, D. C. *Polymer* **2013**, *54*, 702.
10. Zhang, Y. P.; Lee, S. H.; Reddy, K. R.; Gopalan, A. I.; Lee, K. P. *J Appl. Polym. Sci.* **2007**, *104*, 2743.
11. Kim, J. W.; Siochi, E. J.; Carpena-Nunez, J.; Wise, K. E.; Connell, J. W.; Lin, Y.; Wincheski, R. A. *ACS Appl. Mat. Interfaces* **2013**, *55*, 8597.
12. Luong, N. D.; Hippi, U.; Korhonen, J. T.; Soininen, A. J.; Ruokolainen, J.; Johansson, L. S.; Nam, J. D.; Sinh, L. H.; Seppala, J. *Polymer* **2011**, *52*, 5237.
13. Zhitomirsky, I.; Petric, A. *Matter. Lett.* **2000**, *46*, 1.
14. Schaefers, S.; Rast, L.; Stanishevsky, A. *Mater. Lett.* **2006**, *60*, 706.
15. Moon, J. H.; Kim, K. H.; Choi, H. W.; Lee, S. W.; Park, S. *J. Ultramicrosc.* **2008**, *108*, 1307.
16. Tian, Q. H.; Guo, X. Y. *Trans. Nonferrous Met. Soc. China* **2010**, *20*, 283.
17. Liu, S.; Liu, J.; Wang, L.; Zhao, F. *Bioelectrochemistry* **2010**, *79*, 37.
18. Ma, H.; Liu, Z.; Wu, L.; Wang, Y.; Wang, X. *Thin Solid Films* **2011**, *519*, 7860.
19. Leon, C. A.; Aguilar, E. A.; Quintana-Puchol, R.; Drew, R. A. L. *J. Mater. Sci. Lett.* **2002**, *21*, 1375.
20. Beygi, H.; Sajjadi, S. A.; Zebarjad, S. M. *Appl. Sur. Sci.* **2012**, *261*, 166.
21. Wang, H.; Jia, J.; Song, H.; Hu, X.; Sun, H.; Yang, D. *Ceram. Int.* **2011**, *37*, 2181.
22. Reddy, K. R.; Sin, B. C.; Yoo, C. H.; Park, W.; Ryu, K. S.; Lee, J. S.; Shon, D.; Lee, Y. *Script. Mater. 58*, 1010.
23. Chang, H. F.; Saleque, M. A.; Hsu, W. S.; Lin, W. H. (1996). *J. Mol. Catal. A: Chem.* **1996**, *109*, 249.
24. Ge, J.; Zeng, X.; Tao, X.; Li, X.; Shen, Z.; Yun, J.; Chen, J. *J. Appl. Polym. Sci.* **2010**, *118*, 1507.
25. Alsharaeh, E. H.; Othman, A. A.; Aldosari, M. A. *Materials* **2014**, *77*, 5212.
26. Ling, G. P.; Li, Y. *Mater. Lett.* **2005**, *59*, 1610.
27. Silvain, J. F.; Bobet, J. L.; Heintz, J. M. *Compos. Part A* **2002**, *33*, 1387.
28. Xu, H. P.; Dang, Z. M. *Chem. Phys. Lett.* **2007**, *438*, 196.
29. Luyt, A. S.; Molefi, J. A.; Krump, H. *Polym. Degrad. Stab.* **2006**, *91*, 1629.
30. Wei, Y. F.; Li, Z. Q. *Appl. Phys. Lett.* **2013**, *102*, 131911.
31. Choi, S. H.; Kim, D. H.; Raghu, A. V.; Reddy, K. R.; Lee, H. I.; Yoon, K. S.; Jeong, H. M.; Kim, B. K. *J. Macromol. Sci. Part B: Phys* **2012**, *51*, 197.
32. Fu, S. Y.; Feng, X. Q.; Lauke, B.; Mai, Y. W. *Compos. Part B: Eng.* **2008**, *39*, 933.
33. Leong, Y. W.; Bakar, A.; Ishak, Z. A.; Ariffin, A.; Pukanszky, B. *J. Appl. Polym. Sci.* **2004**, *91*, 3315.
34. Kuo, M. C.; Tsai, C. M.; Huang, J. C.; Chen, M. *Mater. Chem. Phys.* **2005**, *90*, 185.
35. Zhou, W.; Qi, S.; Li, H.; Shao, S. *Thermochim. Acta* **2007**, *452*, 36.
36. Krupa, I.; Mikova, G.; Novak, I.; Janigova, I.; Nogellova, Z.; Lednicky, F.; Prokes, J. *Eur. Polym. J.* **2007**, *43*, 2401.
37. Choi, S.; Kim, J. *Compos. Part B: Eng.* **2013**, *51*, 140.
38. Singh, R.; Kulkarni, S. G.; Naik, N. H. *Adv. Mater. Lett.* **2012**, *44*, 82.
39. Lee, J. G.; Kim, S. H.; Kang, H. C.; Park, S. H. *Macromol. Res.* **2013**, *21*, 349.
40. Xie, S. H.; Zhu, B. K.; Wei, X. Z.; Xu, Z. K.; Xu, Y. Y. *Compos. Part A: Appl. Sci. Manuf.* **2005**, *36*, 1152.